The Study of the Elements Migration from the Matrix Phases to the Grain Boundary Effects on the Creep Rupture of G-NiCrTi28W Alloy at Elevated Temperature

Mehrdad Rafiei, Ehsan Saebnoori*

Advanced Materials Research Center, Department of Materials Engineering, Najafabad Branch, Islamic Azad University, Najafabad, Iran.

ARTICLE INFO

Article history:

Received 16 June 2018
Accepted 6 November 2018
Available online 15 June 2019

Keywords:

Heat Resistant Alloy
Creep rupture
Reformer tubes
Modified HV
G4879 Micro

ABSTRACT

The microstructure and mechanical properties of a centrifugally Cast G-NiCrTi28W heat resistant alloy and effects of the elements migration from matrix phase to grain boundary have been stated and the effects of microstructure and composition changes on the life of reformer tubes from a direct reduction iron plant have been assessed. For this purpose, one sample from the as-cast tubes, and one from the aged tubes at 1100 °C for about 8 years, were used. Scanning electron microscopy (SEM) images and energy dispersive spectroscopy (EDS) analysis of two tubes were done. In as-cast tubes, the Cr_7C_3 primary chromium carbides and niobium-tungsten carbides were identified. Aging promoted the occurrence of different phenomena such as the transformation of Cr_7C_3 primary carbides to $Cr_{23}C_6$ secondary carbides, and the transformation of niobium-tungsten carbide to the M_6C tungsten carbides. It was found that aging promoted the reduction in tensile strength from 580 MPa to 100 MPa and the increase in elongation from around 6% to around 30%. According to the results of the creep test at 960 °C and 52 MPa, no rupture occurs on the as-cast reformer tube during the test time.

1-Introduction

The effects of different parameters on ferrate (VI) synthesis through electrochemical methods have been widely studied [1]. Current efficiency and energy consumption are two important factors in sodium ferrate production which play an important role in the determination of the production rate. Anode passivation [2-6], sodium ferrate decomposition [7, 8] and increase in rate of cathodic reactions (e.g. hydrogen reduction [9] and oxygen evolution [2]) [1] in respect to anodic dissolution reaction rate lead to decline in current efficiency and increase the energy consumption in electrosynthesis of sodium ferrate. In all of these studies, the portion of each factor has not addressed to amount of deviations in current efficiency and energy consumption. It is the motivation of this article to determine the effective factors on current efficiency and energy consumption of sodium ferrate synthesis. Iron typically occurs as a metal, or in the valence states Fe (II) or Fe (III), but, more than three stable forms of iron oxidation states of 0, 2 and

Direct reduction iron is an alternative for the production of pure iron. Fig.1 shows the Schematics of the Midrex DRI process where the main features are indicated. In this process with a reducing gas mixture (H_2+Co), the reduction of iron ore (Fe_2O_3) occurs without melting. The production of hydrogen is carried out by steam reforming of natural gas (CH_4) in

* Corresponding author:
E-mail address: saebnoori@pmt.iaun.ac.ir

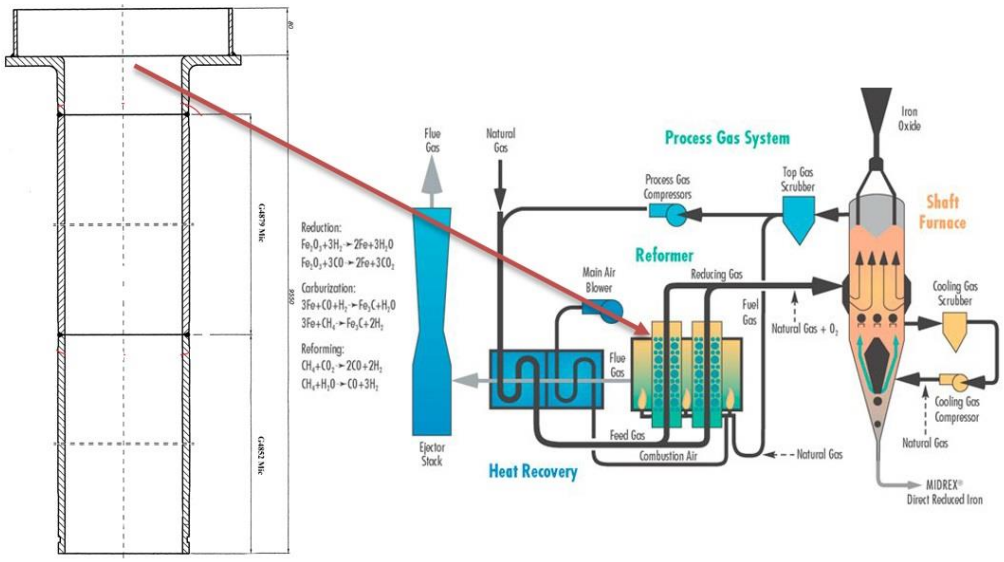

Fig.1. Schematics of the Midrex direct reduction iron process [1].

catalyst-filled tubes. These tubes are Fe-Cr-Ni alloy and have a length of about 9 meters, an internal diameter of 200 mm and wall thickness of 12 mm. This process takes place at an internal pressure of 0.2 MPa and temperature of about 1000-1100 °C [1].

In the direct reduction plant, the best way to increase the reformer capacity is to escalate the operating temperature. Although, this is a simple process and can significantly increase the production, it can reduce the lifetime of the tubes. Over time, due to the high temperature and stress (tube weight), the tubes from the hottest point adjacent to the reformer roof are starting to creep and bulged. At this time, the damaged tube is blocked from the top and bottom and removed from the production cycle during the repair time. For this reason, optimizations have been done on the tubes, but this damage and its effective factors are still very important and can be analyzed [2].

The Fe-Cr-Ni heat resistant alloys do not have heat treatment ability and usually used as casting. These alloys have a good flexibility and due to the high percentage of alloying elements have a good resistant on carburizing and oxidizing atmosphere [3-4].

The influence of alloying elements is one of the important factors in the creep behavior of heat resistant materials. With increasing the percentage of alloying elements, the creep resistance can also be increased. These elements can be effective on the resistance creep by creating primary carbides after the casting [5]. In addition, due to the surge of temperature and the immigration of these elements to the grain boundaries and their transformation to secondary carbides, they have a significant influence on the creeping life of these alloys [6].

In order to arrive at a quantitative estimate of the remaining life of such ageing components, it is necessary to have some hot tensile, creep and stress rupture data for service exposed tubes at high temperature. One of the most widely used techniques for life assessment of components involves the removal of samples and conducting accelerated tests at temperatures above the service temperature [2, 7]. An estimate of the remaining life at the operating hoop stress and temperature is then made by analysis creep rupture data using Larson Miller Parameter (LMP) [7].

This parameter with the aim of connecting the temperature and the rupture time, described by[8]:

$$LMP = T (\log t_r + C) \times 10^{-3} \quad (1)$$

In this relationship, T is the test temperature in Kelvin, t_r is the rupture time in hours and C is the Larson Miller constant which is between 20-30 but is suggested to be about 21.5.

If LMP is evaluated for pairs of time and Temperature obtained over a range stress, a single master curve is obtained for the material (Fig.2). A plot such as this is a good way of summarizing to compare the stress rupture characteristics of several materials [9].

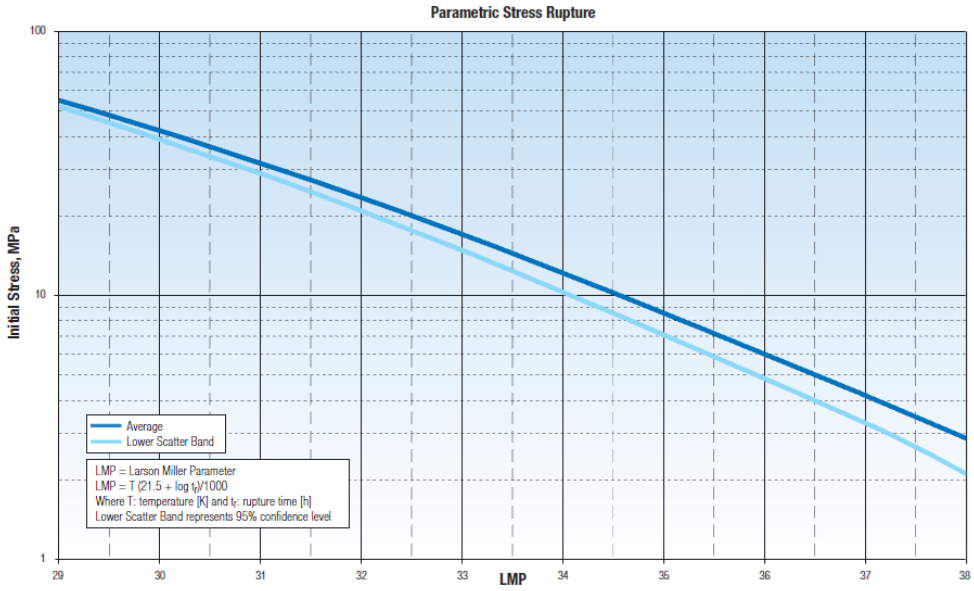

Fig.2. Creep rupture behavior of G-NiCrTi28W [8].

The G-NiCrTi28W alloy, which is a heat resistant alloy casting group, is used to produce reformer furnace tubes in the steel, gas and petroleum industries and specifically in the Mobarakeh Steel Complex. This alloy is also named G4879 Micro and the modified HV heat resistant steel in different industries. G 4879 Micro is a cast austenitic alloy containing nickel, chromium, tungsten and titanium. The alloy has good high temperature stress rupture strength and good carburization and oxidation resistance.

The purpose of this work is to study the changes in the microstructure, grain size and change in the tensile strength of the G-NiCrTi28W alloy after working at high temperatures.

2. Materials and methods

2.1. Preparation and Samples selection

For this study, six reformer tubes of G-NiCrTi28W alloy have been selected, three of them was from new tubes and the other three samples of used tubes with working condition of 1100 °C for 8 years which the aged samples were chosen from maximum creep parts of the top of the tubes.

At first, the tubes were examined macroscopically in terms of dimensions (diameter and thickness) and by general measuring tools and were prepared for the main stages of the research. A schematic of the tube diameter with the selected points is shown in Fig. 3.

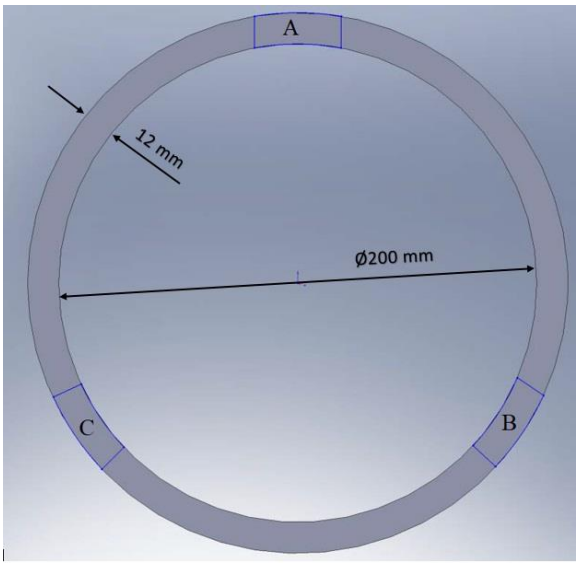

Fig.3. Schematics of the tube diameter.

2.2. Chemical analysis

The chemical composition of the G-NiCrTi28W was determined by means of a BELEC Quantimeter device. The standard chemical composition of G-NiCrTi28W and chemical composition of the aged tube are shown in Table 1 and Table 2.

Table.1. standard chemical composition of G-NiCrTi28W.

Element	C	Si	Mn	S	P	Cr	Ni	W	Ti
Min. wt. %	0.47	0.50	0.40	-	-	28.00	47.00	4.20	0.10
Max. wt. %	0.45	0.80	0.60	0.013	0.010	30.00	49.00	4.60	0.12

Table.2. Chemical composition of aged tube.

Element	C	Si	Mn	Cr	Fe	W	Ti	Ni	Nb	Co	Mo	S
wt. %	0.45	0.55	0.56	28.50	Bal.	3.70	0.053	49.00	0.20	0.035	0.010	0.043

2.3. Microstructure observation

High magnification capability in electron microscopes is effective for accurate observation of carbides and their distribution, which can have a significant impact on the creep behavior of the alloy in the austenitic zones. For this purpose, the microstructure of the specimens is characterized through using Scanning Electron Microscopy (SEM) and Energy Dispersive Spectroscopy (EDS) analysis at the internal, external and middle of the thickness of each tube. The SEM and FESEM images were taken by the VEGA TESCAN-XMU and the (TESCAN-XMU MIRA3) respectively.

2.4. Tensile test

The tensile test at a room temperature for both as cast and aged tubes were performed using Zwick 5111 machine. For this test, three samples with 8.75 mm diameter along the length of different positions as shown as Fig. 3 were prepared according to ASTM A370 [10)] for two tubes. One of the sample prepared shown in Fig. 4.

2.5. Creep Test

In order to study the creep life of as cast tube, a specimen with a diameter of 3.8 mm was prepared according to ASTM A370 [10)] as shown in Fig. 5. The creep tests were performed using SANTAM SCT-30 machine for 30 hours at 960 °C and under the stress of 52 MPa.

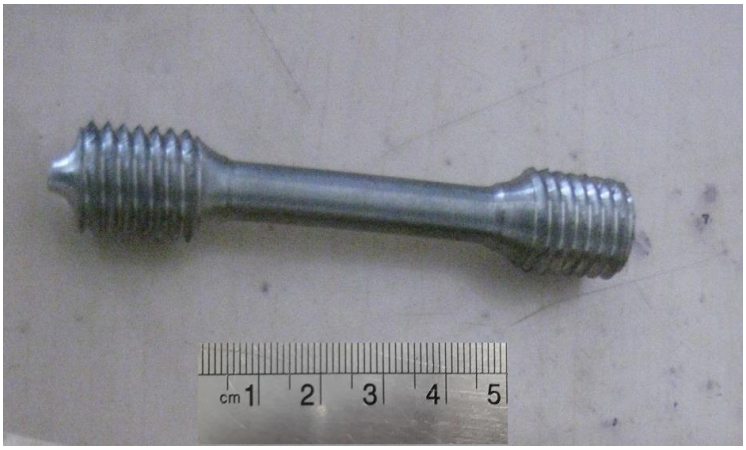

Fig.4. Sample prepared for tensile test.

Fig. 5: Sample prepared for creep test.

3. Results and Discussion

3.1. Chemical analysis results

The modified HV alloy with micro alloy elements exhibits a better creep property than the original alloy (without the elements of titanium and niobium). The creeping strength of this alloy is mainly due to the chemical composition and distribution of the carbide phases or sediment secondary phases during service[11, 12].

According to the results of Table 1, the presence of titanium element can improve the creep resistance of the alloy by forming primary carbides [13]. In addition, due to the high percentage of nickel, it can be concluded that this alloy is austenitic at all temperatures and is not sensitive to the formation of brittle phases[11, 12].

According to Table 1, this alloy has a high percentage of carbon. The variation in the amount of the eutectic carbides is a function of the carbon content of the as cast alloys. Chromium is one of the most important elements in heat-resistant alloys and can increases the oxidation resistance of these alloys. Chromium carbide formation can improve the creep properties of the alloy. In these alloys, the high percentage of tungsten can lead to the formation of tungsten carbide, which is more stable than chromium carbides at temperatures higher than 1100 °C, and have an essential influence on the escalation of the creep strength. Silicon and nickel also has been found to be very effective in improving carburization resistance. The presence of silicon in heat-resistant alloys can have influence on the stability of tungsten carbide [14].

3.2. SEM Study of the as cast tube

The SEM image of the as cast tube is shown in Fig. 6. According to Fig. 6, dark gray phases, light gray phases and inclusion particles are visible on the grain boundary[15]. According to Fig. 7 the EDX analysis, indicated that the dark phase is Cr_7C_3 chromium rich carbides and light gray phase is niobium-tungsten carbides. This brightness contrast is due to the difference in atomic weight of chromium vs. niobium. The black inclusion containing large amounts of sulfur, manganese and chromium are visible on the matrix surface.

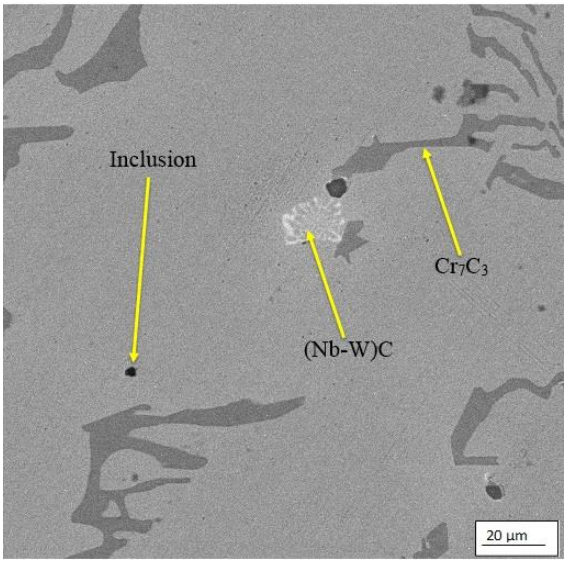

Fig. 6. SEM image of the as cast tube.

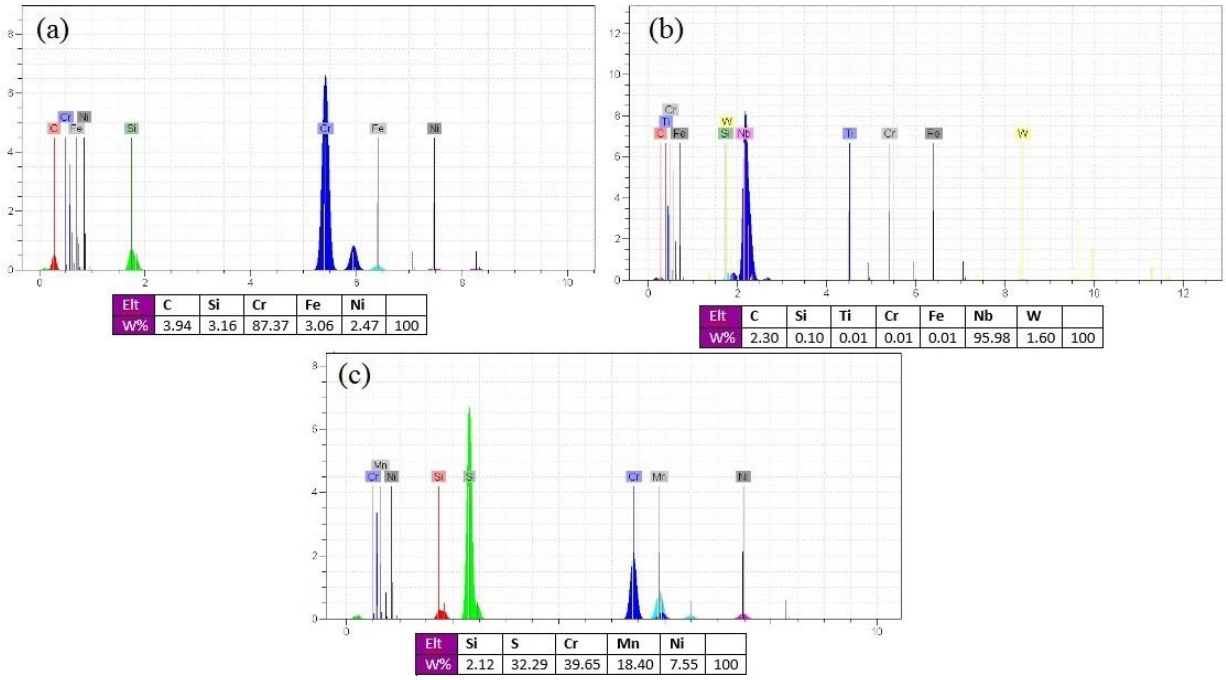

Elt	C	Si	Cr	Fe	Ni	
W%	3.94	3.16	87.37	3.06	2.47	100

Elt	C	Si	Ti	Cr	Fe	Nb	W	
W%	2.30	0.10	0.01	0.01	0.01	95.98	1.60	100

Elt	Si	S	Cr	Mn	Ni	
W%	2.12	32.29	39.65	18.40	7.55	100

Fig. 7. EDS analysis of the as cast tube: (a) dark gray carbides (b) light gray carbides (c) inclusion particles.

Studies show that due to the high carbon content in this alloy and the presence of strong carbide elements, the niobium-tungsten carbides and chromium carbides have been formed[15]. The formation of primary niobium-tungsten eutectic carbides can improve the creep rupture life. Primary eutectic carbides play a main role for preventing the grain boundary slips and limiting the movement of dislocations.

3.3. SEM Study of the thickness middle of aged tube

According to Fig. 8 from the middle of the thickness of aged tube, gray phases, dark gray phases and inclusion particles on the surface of the grains are visible. The dark and light gray phases are continuously sediment on the grain boundary. Comparing the SEM images of aged tube with as-cast tube shows that, the distribution and morphology of the carbides have changed. Based on Fig. 7, the primary carbides have lost their eutectic structure and have become almost coarsened with a blocky shape[15].

The secondary carbides coarsened can change the mechanical properties of the alloy, reduced the creep strength, and increase the alloy's flexibility[13].

EDS analysis of phases are shown in Fig.9. According to analyze of dark gray carbides, it has been determined that during the aging, the

Cr_7C_3 carbides transform into $Cr_{23}C_6$ carbides. Based on this result, it is characterized that the carbon and chromium elements immigrate to the grain boundary by forming a new carbides[16]. Also, according to the EDS analysis, the light gray phases are the secondary tungsten-rich carbides M_6C along the grain boundary could be observed within the grain, inclusion particles. No G-phase ($Ni_{16}Nb_6Si_7$) or γ' phase is found in this alloy[17]. It was pointed out that the amount of silicon more than 1.6 wt. % promotes the formation of G-phase by facilitating the conversion of NbC. Less than 1.5 wt. % silicon in the G-NiCrTi28W alloy may be the reason of the nonexistence of niobium intermetallic.

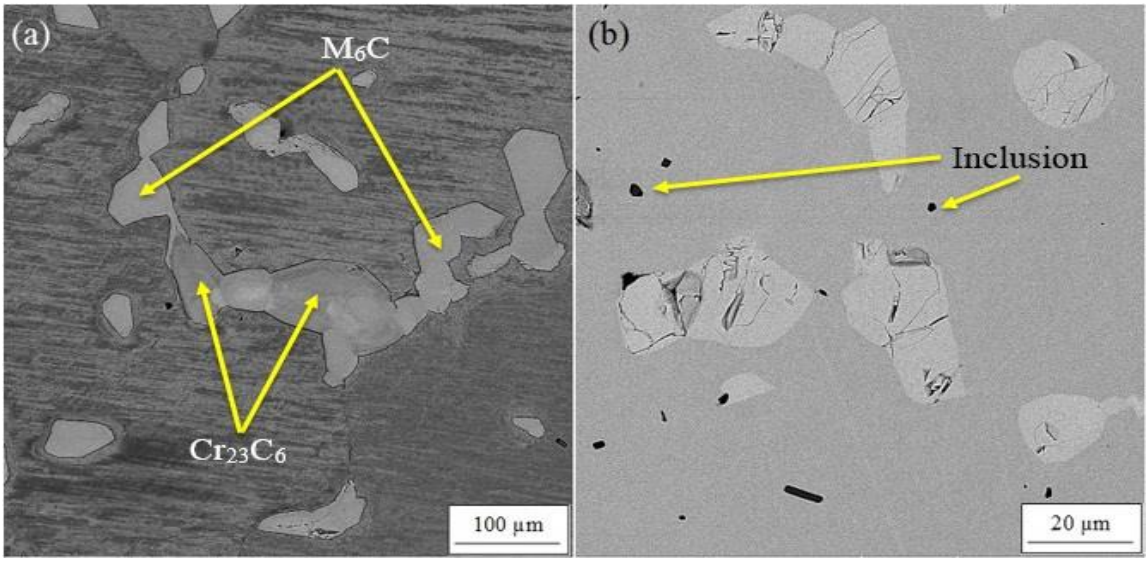

Fig. 8(a, b). SEM images of the thickness middle of aged tube at different magnifications.

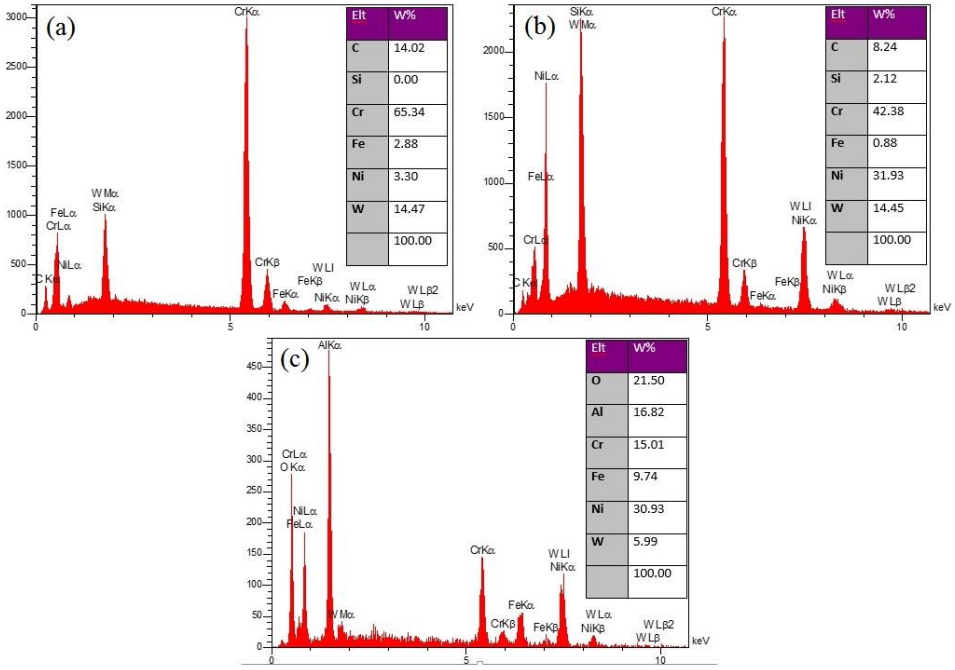

Fig. 9. EDS analysis of the aged tube: (a) dark gray carbides (b) light gray carbides (c) inclusion particles.

3.4. SEM Study of the inner surface of aged tube

The SEM images of the inner surface of aged tube are shown in Fig. 10. In these images, dark and light gray phases and inclusion particles are visible. In Fig. 10a, it is observed that the morphology and distribution of the carbides are different from the middle of the tube thickness. The inner surface of the reformer tube is in the low temperature than the outer surface. Due to the structure type and service environment, the carbides morphology and distribution are greatly different between inner and outer wall and the shape of carbides are not complete blocky[15].

The important point shown in Fig. 10b is the appearance of creeping cavities. These cavities are visible in very small size near the inner surface.

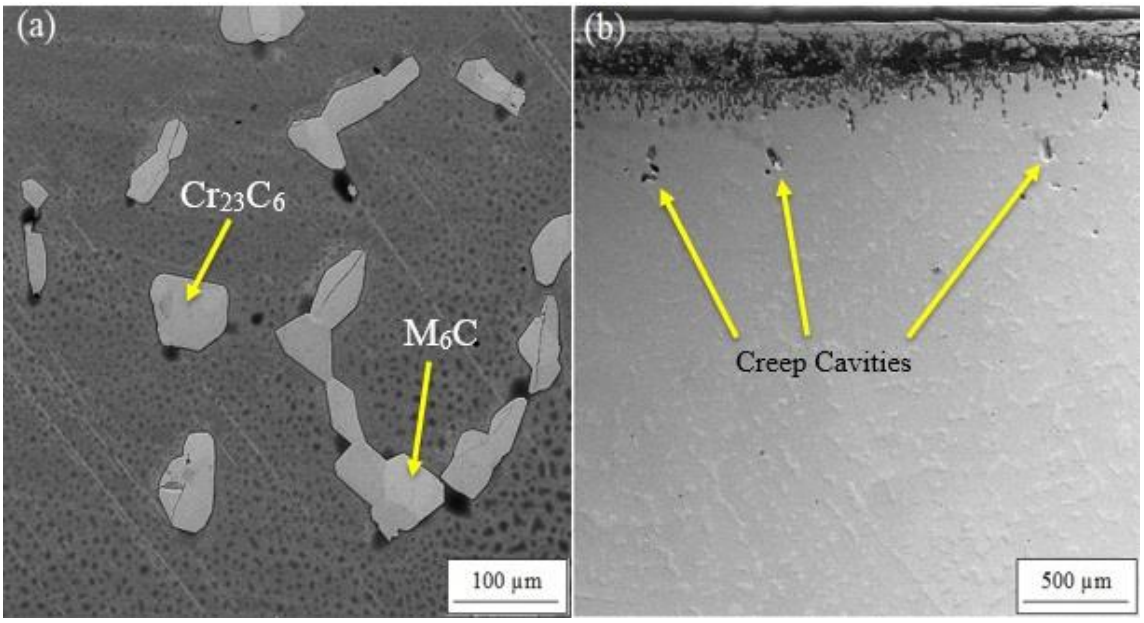

Fig. 10. (a) SEM image of the inner surface of aged tube (b) SEM image of creep cavities.

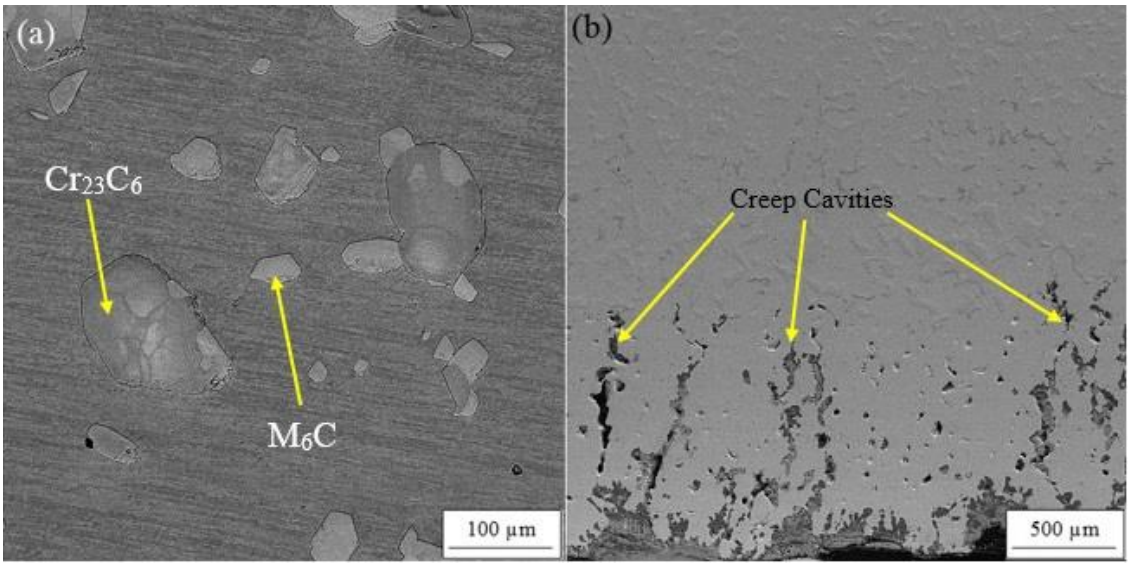

Fig. 11. (a) SEM image of the outer surface of aged tube (b) SEM image of creep cavities.

3.5. SEM Study of the outer surface aged tube

Figure 11 shows the SEM images of the outer surface of the aged tube. As seen in Fig. 11a, the morphology and distribution of secondary carbides on the grain boundary are very different from the inner surface. In these images, the size of the carbides are very coarse with a blocky shape[15, 16]. In addition, their distribution is not uniform and continuous. In Fig. 11b, many creeping cavities near the outer surface have grown inside of the wall.

3.6 Compare samples according to carbide size regards

The carbide sizes in SEM images of inner, middle and outer surface of aged tube were shown in Fig.12. Average dimension of carbides sizes were presented in the Table 3. According to this information, it can be concluded that the M_6C carbides size from the inner surface to the outer surface of tube has decreased and the $Cr_{23}C_6$ carbides size from the inner surface to the outer surface of tube has increased and the carbides were very coarse with a blocky shape [16].

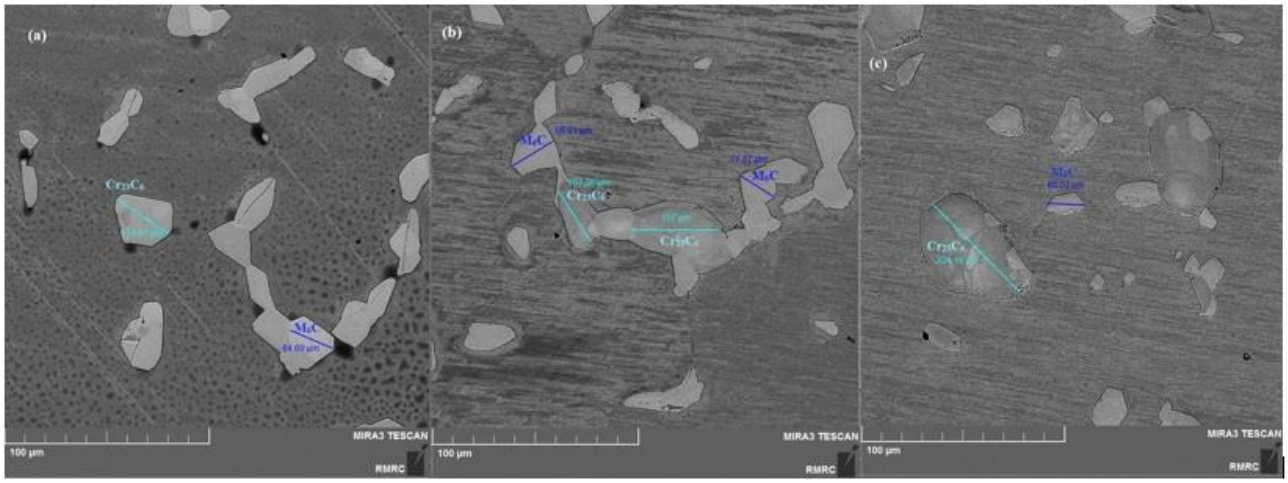

Fig. 12. Carbide size of the aged tube: (a) inner surface (b) middle surface (c) outer surface.

TABLE3: Average dimension of carbides sizes of the aged tube.

Position of test	$Cr_{23}C_6$ (µm)	M_6C (µm)
Inner surface	112.6	84.69
Middle surface	132.19	79.24
Outer surface	224.15	66.07

3.7. Tensile test

The mechanical properties at room temperature of the as cast and aged tubes were presented in the Tables 4 and Tables 5.

Table 5 shows that the aging process affects the mechanical properties. The aging treatment promoted reduction in tensile strength from around 580 MPa to around 100 MPa and the increment in elongation from around 6% to around 30%. This can be due to the morphology of secondary carbides as shape as blocky carbides[11].

Table 4. Mechanical properties of the as cast tube at room temperature.

Position of test	Tensile strength (MPa)	Yield strength (MPa)	Elongation (%)
A	493	374	7
B	488	365	6
C	543	383	7

Table 5. Mechanical properties of the aged tube at room temperature

Position of test	Tensile strength (MPa)	Yield strength (MPa)	Elongation (%)
A	91	74	28
B	93	77	29
C	118	95	33

3.8. Creep test

In order to study the creep resistance of the as cast tube, a creep rupture strength test was performed on it. The results of this test are listed in Table 6. Dispersion of fine particles carbides or intermetallic in the austenite matrix can result in high creep strength[11]. Nb and Ti are presented in form of carbides and nitrides to optimize the structure of grain boundary; and the rare-earth element boron can suppress the silicon trapped at the grain boundary and cause the oxygen segregation. Previous study[11] also showed that larger amounts of carbide typically result in improved creep properties and that the presence of both $M_{23}C_6$ and MC carbides are beneficial

Table 6. Creep rupture strength of the as cast tube at elevated temperatures.

Stress (MPa)	Temperature (°C)	Time (h)	Elongation)%(	LMP	Result
52	960	30	3.15	15.78	Not rupture

for high temperature creep properties[11]. By studying the results of the creep test, comparing and inserting the data of Table 6 in the Larson Miller relationship, it is found that the alloy used in the Mobarakeh Steel Reformer Tubes has the low creep rupture resistance.

3.9. Determine the mechanism of creep

In the SEM images obtained from the aged tube, creeping cavities were observed. Fig. 13 shown an image of the cavities in this tube.
Wedge shape cracks which mostly initiate at the grain boundaries are aligned for maximum shear as shown in Fig. 13 [8]. In this picture, we can see the grain boundary sliding (GBS) under different direction of forces. In this study, due to the weight force, the GBS occurs as shown in Fig.14b. They initiate by grain boundary sliding in the manner illustrated in Fig.14. A commonly used illustration of a wedge type crack initiation by GBS, its formation and growth (first presented by Chang and Grant, and found in almost every publication) is shown in Fig. 14[18]. A number of wedge type crack configurations have been experimentally observed at triple points. Wedge type crack formation at triple points was initially suggested by Zener as early as 1948. According to Zener, at sufficiently high temperatures, grain boundaries behave in a viscous manner and, when near triple points under an applied tensile stress, wedge-type cracks develop due to the high stress concentration. Specifically, Zener was among the first to suggest the concept that fracturing is a consequence of plastic deformation, which is required for crack formation[18].

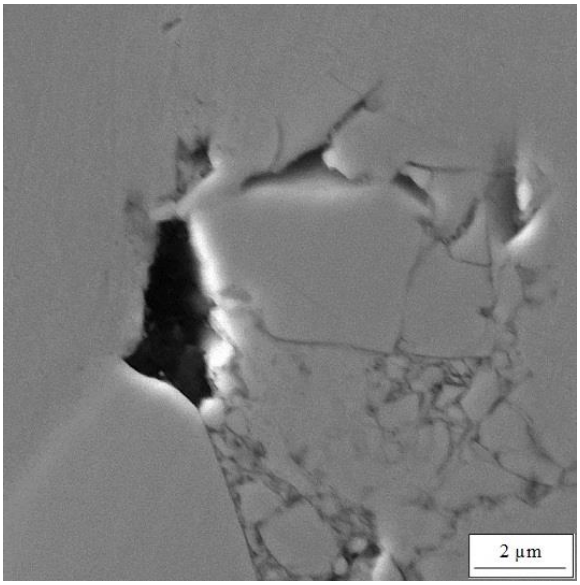

Fig. 13. SEM image of creep cavities of the aged tube.

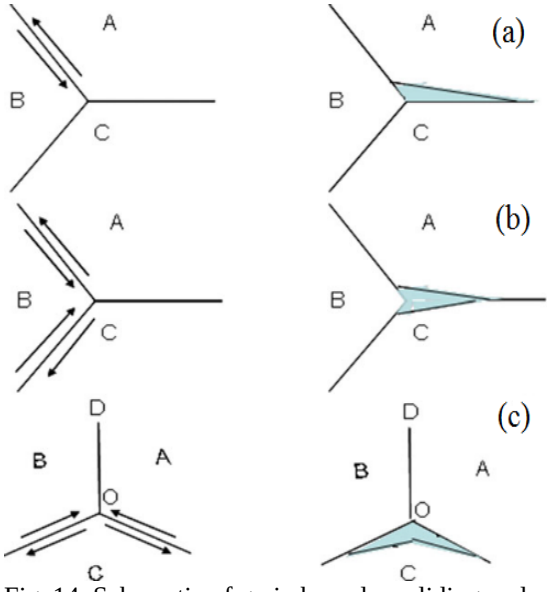

Fig. 14. Schematic of grain boundary sliding under different direction of forces [8].

4. Conclusion

The microstructure of the G-NiCrTi28W used in the as cast reformer tube is composed by austenitic matrix and a network of primary carbides present in the grain boundaries. The scanning electron microscopy image reveals that the carbides are from two different types. EDX microanalysis showed that Niobium-Tungsten carbides appear with color of bright gray, whereas chromium rich Cr_7C_3 appears in dark gray. Aging for about 8 years at 1100 °C produced changes in the morphology and chemical composition of the primary phases and the precipitation of secondary $Cr_{23}C_6$ carbides. It was found that the Cr_7C_3 primary carbides were transformed into blocky shape $Cr_{23}C_6$ secondary carbides, and that the niobium-tungsten carbides transformed into the M_6C. By comparing the samples according to carbide size, the M_6C carbides size from the inner surface to the outer surface of tube has decreased and the $Cr_{23}C_6$ carbides size from the inner surface to the outer surface of tube has increased.

Aging affected the mechanical properties of the material, the main effects were the increase of the elongation and as a result, increase in the ductility and finally changes in the dimensions and shape of the tubes. The aging treatment promoted reduction in tensile strength from around 580 MPa to around 100 MPa and the increment in elongation from around 6% to around 30%.

The rupture creep test results for as cast tube at 960 °C and 52 MPa for 30 hours, have shown that the creep rupture does not occur. By comparing the results with Larson Miller parameter, it was found that the G-NiCrTi28W alloy used in the Mobarakeh Steel Complex reformer tubes has a low creep rupture strength.

References

[1] Q. Ponce. A. Oscar: Structural and Magnetic Studies of an Ex-service Cast Austenitic Steel Tube Used in Hydrogen Reformers, Vol.74, University of Illinois at Chicago, (2012), 194.
[2] N. Roy, A. Raj, B.N. Roy, & A. K. Ray: Can. Metall. Q., 54, (2015) 205.
[3] M. Garbiak, W. Jasiński, & B. Piekarski: Arch. Found. Eng. 2, (2011), 47.
[4] A. Drotlew, M. Garbiak, & B. Piekarski: Arch. Found. Eng. 12, (2012) 31.
[5] M. Shademani, M.R Rahimipour, A. Sedaghat, M. Farvizi: J. Mat. Pro. 4, (2017), 66.
[6] M. Attarian, M., and A. Karimi Taheri.: Mater. Sci. Eng. A, 659, (2016), 104.
[7] A. K. Ray, Y. N. Tiwari, P. K. Roy, S. Chaudhuri, S. C. Bose, R. N. Ghosh, & J. D., Whittenberger,: Mater. Sci. Eng. A, 454, (2007), 679.
[8] G.E. Dieter: Mechanical Metallurgy, David Bacon, London, (1988).
[9] Schmidt Clemens Group: Centralloy G4879 Micro material data sheet, (2010).
[10] ASTM Standard A370: Standard Test Methods and Definitions for Mechanical Testing of Steel Products, (2006).
[11] D. Kong, X. Zhang: MSAIJ, 11, (2014), 36.
[12] F.S. Yin, L. Q. Tian, B. Xue, X. B. Jiang & L. Zhou: metallurgical and materials transactions, A, 43, (2012), 2203.
[13] R.M.T. Borges, L.H. Almeida, T.D. Silveria, & M. Le: Mater. Charact. , 29, (1992), 387.
[14] G.Y. Lai: High Temperature Corrosion and Material Applications, ASM International, (2007).
[15] A. K. Ray, S. Kumar, G. Krishna, M. Gunjan, B. Goswami, S. Chandra Bose: Mater. Sci. Eng. A, 529, (2011), 102.
[16] R. Voicu, E. Andrieu, D. Poquillon, J. Furtado, J. Lacaze: Materials characterization, 60, (2009), 1020.
[17] W. Z. Wang, F.Z. Xuan, Z.D. Wang, B. Wang, C.J. Liu: Materials and design, 32, (2011), 4010.
[18] J. Pelleg: Springer International Publishing, (2017), 445.